nature structural & molecular biology

Mapping the sequence of conformational changes underlying selectivity filter gating in the $K_v11.1$ potassium channel

David T Wang[1–3], Adam P Hill[1–3], Stefan A Mann[1,2], Peter S Tan[1] & Jamie I Vandenberg[1,2]

The potassium channel selectivity filter both discriminates between K^+ and sodium ions and contributes to gating of ion flow. Static structures of conducting (open) and nonconducting (inactivated) conformations of this filter are known; however, the sequence of protein rearrangements that connect these two states is not. We show that closure of the selectivity filter gate in the human $K_v11.1$ K^+ channel (also known as hERG, for ether-a-go-go–related gene), a key regulator of the rhythm of the heartbeat, is initiated by K^+ exit, followed in sequence by conformational rearrangements of the pore domain outer helix, extracellular turret region, voltage sensor domain, intracellular domains and pore domain inner helix. In contrast to the simple wave-like sequence of events proposed for opening of ligand-gated ion channels, a complex spatial and temporal sequence of widespread domain motions connect the open and inactivated states of the $K_v11.1$ K^+ channel.

The ion conduction pathway of K^+ channels is coincident with the central axis of the functional tetramer[1], with the pore domain of each K^+ channel subunit composed of an outer helix, an inner helix and a pore helix that supports the selectivity filter (see **Fig. 1a**). Gates located at the intracellular and/or extracellular entrances to the pore control ion conduction[2]. The intracellular gate is usually referred to as the activation gate and controls transitions between the closed and open state of the channel. Gating at the extracellular entrance to the pore is sometimes referred to as collapse of the pore gating[2] or selectivity filter gating[3] and controls transitions between the open state and the inactivated state, another nonconducting state distinct from the closed state.

A complete understanding of ion channel function requires knowledge of the structures and relative energies of the stable end states as well as the transition-state ensembles that define the energetic barriers between them[4]. These energy relationships can be summarized in the form of a reaction coordinate diagram where the stable states are shown to occupy the energy wells and the transition-state ensembles are depicted as energy barriers (see **Fig. 1b**). Although X-ray crystallography has defined the structures of some of the static, stable endpoints for ion channels[1,5–7], the short-lived, high-energy transition-state ensembles are not amenable to direct structural analysis[8–10].

The only way that the energetics of transition-state ensembles can be investigated experimentally at present is by studying the kinetics of conformational changes[8–10]. The critical question then becomes how one can relate kinetic measurements to the structural changes that are taking place in the protein. Over the last two decades, the method of Φ-value analysis has been adapted to address this precise problem[8–10]. Φ-value analysis involves examination of systematic perturbations on the kinetic and thermodynamic relationships between two stable end states. Specifically, a Φ value is calculated from the ratio of the perturbation to the energetics of the transition state $\Delta\Delta G^{\ddagger}$ relative to that of the ground states (open and inactivated) of the reaction $\Delta\Delta G^0$ (see **Fig. 1**), as in equation (1):

$$\Phi = (\Delta G^{\ddagger}_{WT} - \Delta G^{\ddagger}_{p}) / (\Delta G^{0}_{WT} - \Delta G^{0}_{p}) \quad (1)$$

where WT denotes the wild-type protein and p denotes the perturbed protein.

In theory, Φ-value analysis can be applied to any two-state process—that is, any process in which there are two ground states separated by a single transition state[8–10]. For a two-state reaction, Φ values between 0 and 1 have been interpreted as indicating the extent to which the local structure in the transition state, which is affected by the perturbation, resembles the local structure in the end states; in other words, a Φ value close to 0 indicates that the local structure in the transition state at the point of perturbation resembles the local structure of that region in the initial state, whereas a Φ value close to 1 indicates that it resembles the local structure of that region in the final state[8,9,11]. Φ values have also been interpreted as indicators of the temporal sequence of domain motions underlying the interconversion between two conformational states, where Φ values close to 1 indicate earlier steps in the reaction and Φ values close to 0 indicate later steps in the reaction[12–14].

In this study we have used Φ-value analysis to probe the dynamics of inactivation gating in the $K_v11.1$ potassium channel, encoded by

[1]Mark Cowley Lidwill Research Program in Cardiac Electrophysiology, Molecular Cardiology and Biophysics Division, Victor Chang Cardiac Research Institute, New South Wales, Australia. [2]St. Vincent's Clinical School, Faculty of Medicine, University of New South Wales, New South Wales, Australia. [3]These authors contributed equally to this work. Correspondence should be addressed to J.I.V. (j.vandenberg@victorchang.edu.au).

Received 9 May; accepted 18 October; published online 19 December 2010; doi:10.1038/nsmb.1966

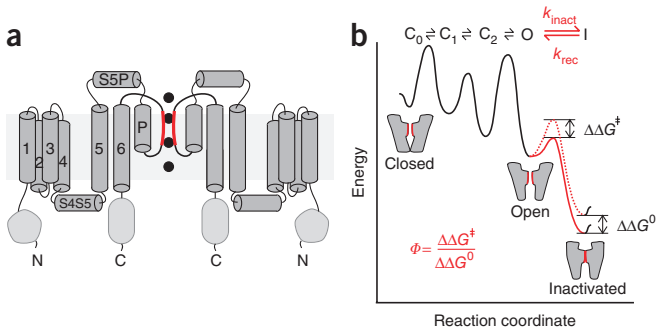

Figure 1 Schematic representation of topology and energetics of gating in $K_v11.1$ channels. (**a**) Topology of $K_v11.1$ channel showing two of the four subunits. The central ion conduction pore lined by the selectivity filter (red) with K^+ ions shown as black spheres. Individual domains are numbered on the left hand subunit. (**b**) Reaction co-ordinate diagram for $K_v11.1$ channel gating. The transition from the closed (C) to open (O) state involves at least three kinetically distinct closed states, whereas the transition from the open to inactivated (I) state contains a single dominant transition state (red segment of trace)[25]. The dashed red line shows the effect of a perturbation that affects both the energetics of the transition state $\Delta\Delta G^{\ddagger}$ as well as the energy difference between the open and inactivated states, $\Delta\Delta G^{0}$.

the human ether-a-go-go–related gene. Understanding the molecular and structural basis of $K_v11.1$ inactivation gating is of considerable clinical and pharmaceutical interest, as this process is critical for normal cardiac repolarization. Disruption to inactivation gating in $K_v11.1$ results in a markedly increased risk of cardiac arrhythmias and sudden cardiac death[15]. $K_v11.1$ inactivation is also a major contributor to the promiscuity of drug-binding to the channel[16], resulting in the unintended side effects of arrhythmia and sudden death observed among users of many prescription drugs[15]. Inactivation of $K_v11.1$ involves collapse of the selectivity filter[17,18]. However, the mechanism underlying inactivation is likely to be much more complex than just collapse of the selectivity filter, given that $K_v11.1$ is affected by mutations in multiple domains throughout the channel[17,19–23]. Here, for the first time, we apply the technique of *Φ*-value analysis to the study of a K^+ channel. We demonstrate that the interconversion of the conducting and nonconducting conformations of the selectivity filter in $K_v11.1$ proceeds via a complex series of consecutive moves involving rearrangements of extracellular, transmembrane and cytoplasmic domains, analogous to the process of opening and closing a Japanese puzzle box.

RESULTS

Application of *Φ*-value analysis to $K_v11.1$ inactivation

Φ-value analysis can be applied to processes dominated by a single transition state. Inactivation in $K_v11.1$ is both rapid and voltage dependent[17,18,24]. These properties make it relatively easy to isolate the open-inactivated state transition from the closed-open state transitions (which are considerably slower)[17,25]. It has, however, been shown that $K_v11.1$ channels can transit from pre-open closed states directly to an inactivated state[26]. There is also likely to be more than one inactivated state[27], and there may be multiple distinct open states of the channel[28]. We therefore sought to determine under what conditions transitions between 'open states' and 'inactivated states' are dominated by a single dominant transition state and so are amenable to *Φ*-value analysis. We used voltage protocols that ensured the voltage sensor of the channels was in the open conformation and, where necessary, accounted for any deactivation that might occur before complete recovery from inactivation at hyperpolarized potentials (see **Fig. 2a**); in other words, we restricted our analysis to what we call open-state inactivation, the process that is critically involved in the termination of the cardiac action potential. Under these conditions, a plot of the logarithm of the observed rate constants of inactivation and recovery from inactivation versus voltage shows the typical chevron shape (**Fig. 2b**) observed for reactions with a single dominant transition state between the two end states[29]. From the derived values for the rate of inactivation k_{inact} and recovery from inactivation k_{rec}, one can calculate an equilibrium constant:

$$K_{inact,V} = k_{inact,V} / k_{rec,V} \quad (2)$$

where V refers to the voltage at which measurements were made.

We also estimated the equilibrium constant for inactivation by plotting the amplitude of the steady-state plateau current versus the peak current at each voltage (**Fig. 2a**,**c**). The two methods for calculating the equilibrium constant gave almost identical answers for WT channels (**Fig. 2c**) and mutant channels (see **Supplementary Fig. 1**), which is consistent with the idea that the transition from open state to inactivated state is dominated by a single major transition state.

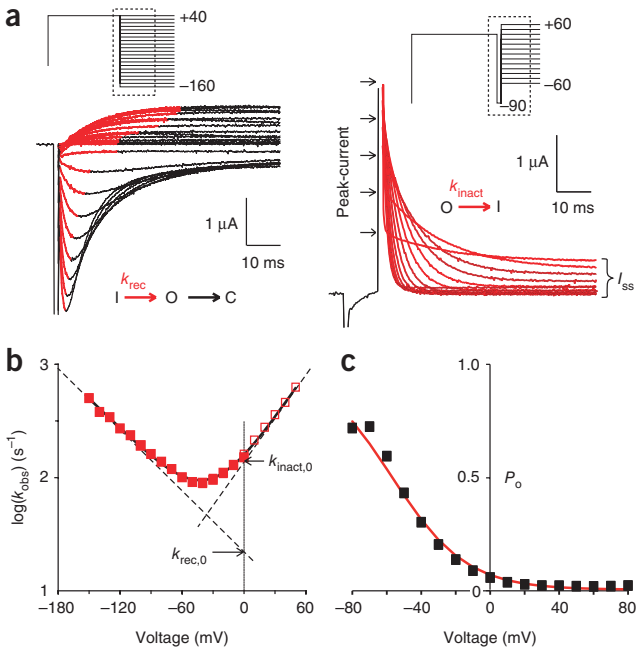

Figure 2 Measurement of inactivation in $K_v11.1$ channels. (**a**) Measurement of rates of recovery from inactivation using double-pulse protocol (left) and rates of inactivation using triple-pulse voltage protocol (right). Portions of the current traces in red indicate the sections used to measure rates of recovery from inactivation (left) and rates of inactivation (right). On right panel, arrows indicate peak currents and I_{ss} indicates steady-state current levels that were used to calculate equilibrium values for inactivation (see panel **c**). (**b**) A plot of the logarithm of the observed rate constants of inactivation (red unfilled squares) and recovery from inactivation (red filled squares) versus voltage shows the typical chevron shape observed for reactions with a single dominant transition state between the two end states[29]. The solid line is a fit of equation (3) (Online Methods), $k_{obs,V} = k_{inact,V} + k_{rec,V}$, and the dashed lines are the derived unidirectional rate constants $k_{inact,V}$ and $k_{rec,V}$. The values for $k_{inact,V}$ and $k_{rec,V}$ at 0 mV, highlighted on the graph, are used to calculate the equilibrium constant at 0 mV: $K_0 = k_{inact,0} / k_{rec,0}$. (**c**) Comparison of the equilibrium constant for inactivation, calculated using the ratio of $k_{inact,V} / k_{rec,V}$ (red line), with the ratio of steady-state current to peak current from the right hand graph in **a** (black squares).

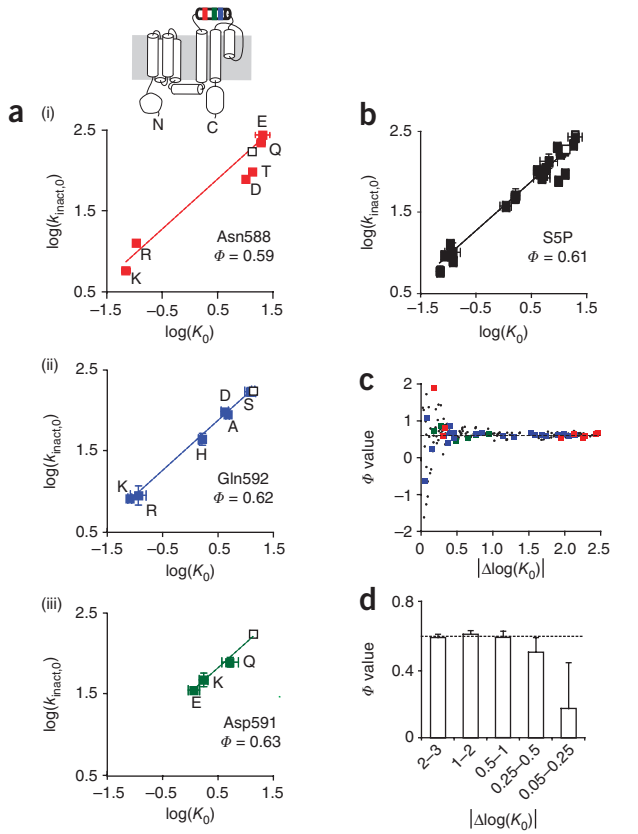

Figure 3 Mutations in the outer turret affect energetics of $K_v11.1$ inactivation. (**a**) Plots of $\log(k_{inact,0})$ versus $\log(K_0)$ for mutations in the amphipathic α-helix in the S5P domain: (i) Asn588, (ii) Gln592 and (iii) Asp591. Color coding refers to location of mutated residues on topology diagram. Individual mutations are indicated by their single-letter amino acid codes. In each panel, the unfilled square shows WT $K_v11.1$ and error bars are ± s.e.m. for $n = 3$–8 oocytes. In some instances, error bars are within the symbols. (**b**) Summary plot showing all mutations for all residues in the S5P linker (see also **Supplementary Table 1**). (**c**) Plot of Φ value versus $|\Delta\log(K_0)|$ for each pair of mutants in the S5P domain. Colored squares depict pairs of mutants that both occur in Asn588 (red), Gln592 (blue) or Asp591 (green). The dashed line indicates the Φ value from **b**. (**d**) Plot of mean Φ values for pairs of mutants where the absolute value of $\Delta\log(K_0)$ lies in the ranges indicated. The dashed line indicates the Φ value from **b**. When $\Delta\log(K_0)$ is small, even small errors in the measurement of $\Delta\log(K_0)$ can lead to large errors in the calculated Φ value. $\Delta\log(K_0)$ needs to be > 0.5 to obtain an accurate estimate of Φ values.

The interpretation of Φ values, when applied to conformational changes in complex systems such as proteins, is predicated on the assumption that mutations do not perturb the structure of the ground states, nor do they alter the pathway between the two ground states[8,14] (see **Supplementary Fig. 2**). Therefore, as an additional safeguard, we restricted our analysis to mutant channels that retained high selectivity for K^+ over Na^+, because reduced selectivity is associated with a separate slow inactivated state[27], which could introduce uncertainty into our analysis.

Conformational changes around the selectivity filter

We first examined the effect of mutations in the turret region immediately extracellular to the selectivity filter, as mutations in this region have been shown to have dramatic effects on selectivity filter gating in a wide range of channels[23,30–32]. In $K_v11.1$ channels, this turret is formed by a 40-amino-acid loop between the S5 and pore helices, the so-called S5P linker[20,22]. Asn588 in the S5P linker was mutated to arginine, lysine, aspartate, glutamate, serine and threonine. The maximum $\Delta\log(K_0)$ among these mutants was 2.26 log units, well above the threshold of 0.5 log units required to obtain reliable Φ-value measurements[33] (see Online Methods and **Fig. 3**). The mean Φ value for mutants of Asn588 was 0.59 (see **Fig. 3a**). When we coexpressed N588R and WT subunits at different ratios, the plot of $\log(k_{inact,0})$ versus $\log(K_0)$ gave a straight line with a slope of 0.55 (see **Supplementary Fig. 3**), similar to that obtained for N588R alone compared to WT. This suggests that each of the four subunits contributes equally (~50-fold decrease in the equilibrium for each mutant subunit) to the energetics of inactivation.

Asn588 is located on an amphipathic α-helix in the S5P linker[22]. This amphipathic α-helix contains a glycine residue located at approximately the midpoint (Gly590). To investigate whether the second half of the helix might move independently of the first half of the helix, we introduced mutations at other residues in the S5P α-helix. The Φ values for mutations introduced at Asp591 and Gln592 were very similar to that measured for Asn588, which was about 0.6 (**Fig. 3a**). Further, the Φ value obtained from a linear regression of the $\log(k_{inact,0})$ versus $\log(K_0)$ data for all S5P mutants was 0.61 (see **Fig. 3b**). This suggests that the entire S5P amphipathic α-helix moves synchronously during $K_v11.1$ inactivation. We did not analyze mutants of the hydrophobic residues in the S5P α-helix or those with hydrophobic residues replacing polar residues, as previous studies from our laboratory[22] and others[20] have shown that these mutants are invariably either associated with loss of selectivity for K^+ relative to Na^+ ions or not expressed.

We next looked at mutations to Ser631 in the PS6 linker (equivalent to Thr449 in Shaker), a residue that has previously been shown to play a major role in inactivation, in both $K_v11.1$ channels[23] and Shaker K^+ channels[34]. Ser631 was mutated to alanine, tyrosine, histidine, cysteine, glutamine, glutamate and asparagine. The last three had abnormal selectivity and so were not studied further. The mean Φ value for WT, S631A and S631Y was ~0.25. S631C and S631H gave anomalous Φ values (8.3 and −7.5, respectively): that is, they showed large changes in $k_{inact,0}$ (and $k_{rec,0}$) with minimal change in K_0, which is analogous to the effect of a catalyst[35]. This suggests that these mutations have stabilized (S631C) or destabilized (S631H) the transition state (see **Supplementary Fig. 2**) and so will have altered the transition pathway between the open and inactivated states[8,36]. Accordingly, data for these mutations were excluded from the analysis depicted in **Figure 4a**. No other residues in the PS6 linker had max $\Delta\log(K_0)$ values >0.5. Nevertheless, a plot of all the PS6 mutants studied (see **Supplementary Table 1** for a list of all mutants examined) gave a Φ value of 0.26, very similar to that for Ser631 alone.

Three out of 23 mutants introduced to residues in the selectivity filter or the linker between the pore-helix and the selectivity filter (between residues Ser621 and Asn629; see **Supplementary Table 1** for a list of all mutants examined) resulted in channels that did not perturb the native state and did not have anomalous Φ values (see **Fig. 4b**). These were S621A at the distal end of the pore helix, T623S between the pore-helix and selectivity filter and V625T at the intracellular entrance to the selectivity filter. These residues had Φ values of ~0.26 (see **Fig. 4b**). Taken together, these data suggest that $K_v11.1$ inactivation involves conformational changes in the extracellular turret that precede conformational changes in the vicinity of the selectivity filter.

Conformational changes remote from the selectivity filter

Recent work on KirBac 3.1 (ref. 5) and KcsA[6,37] potassium channels has shown that in addition to being coupled to conformational changes in the immediate vicinity of the selectivity filter, inactivation

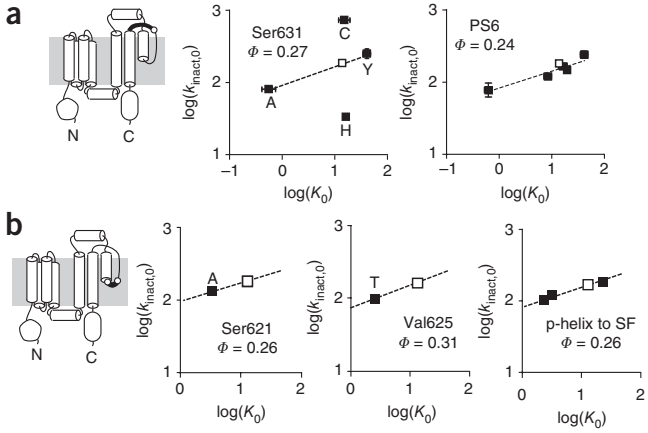

Figure 4 Mutations adjacent to the selectivity filter affect a late step in $K_v11.1$ inactivation. (**a**) Plots of $\log(k_{inact,0})$ versus $\log(K_0)$ for residues in the linker between the selectivity filter and S6. Left, plots for individual residues where max $\Delta\log(K_0)$ is > 0.5; right, summary plot for all mutants in the domain. (**b**) Plots of $\log(k_{inact,0})$ versus $\log(K_0)$ for the linker between the pore-helix (p-helix) and selectivity filter (SF). Left and middle, plots for individual residues (mutations are indicated by their single-letter amino acid codes); right, summary plot for all residues. In each panel, the unfilled squares show WT $K_v11.1$, and error bars are ± s.e.m. for n = 2–8 oocytes. In some instances error bars are within the symbols. White dots in the topology diagrams at far left indicate the approximate location of residues highlighted in left panels of each row. For purposes of clarity, individual mutations are not identified in the summary plots on right of each row, but the properties of all mutants examined are summarized in **Supplementary Table 1**.

is coupled to widespread conformational changes, including to changes in transmembrane as well as cytoplasmic domains of the channel. Although the structural and spectroscopic methods used in these studies reveal that distal domains are associated with selectivity filter gating, they cannot tell us what point in the inactivation process involves these domains, so the mechanistic insight they provide is limited.

We therefore extended our Φ-value analysis of $K_v11.1$ inactivation to the pore domain transmembrane helices. In the inner helix of the pore domain (S6), mutations to Val644 resulted in a Φ value of 0.31 (see **Fig. 5a**). The two residues with informative Φ values in the outer helix of the pore domain (S5: Leu564 and Leu550) both had Φ values of ~0.75 (see **Fig. 5b**). Thus, the outer helix of the pore domain must move substantially earlier than the inner helix of the pore domain.

In the cytoplasmic S4-S5 linker, which has been shown to couple voltage sensor movement to the opening of the intracellular activation gate[7,38], we identified two informative mutants, Asp540 and Ser543, both of which had Φ values of ~0.4 (see **Fig. 5c**). This indicates that during the transition from the open to inactivated states, changes to the conformation of the S4-S5 linker occur after changes to the outer helix of the pore domain but precede changes to the inner helix of the pore domain.

The one remaining break in our communication pathway is between the extracellular S5P domain (Φ ~ 0.6) and the intracellular S4-S5 linker (Φ ~ 0.45). The intervening S5 domain has a Φ value of ~ 0.75, so it cannot provide the link. We therefore investigated whether the voltage sensor domain might do so. None of the residues in the S4 domain that we examined had $\Delta\log(K_0)$ values > 0.5 (see **Supplementary Table 1**). However, a plot of $\Delta\log(k_{inact,0})$ versus $\Delta\log(K_0)$ for all 25 mutants gave a Φ value of 0.54, with the maximum $\Delta\log(K_0)$ between any two mutants in the S4 domain being 0.72 (see **Fig. 5d**). A Φ value of 0.54 is consistent with the idea that the S4 domain provides a link between the extracellular S5P domain and the intracellular S4-S5 linker.

K^+ exit from the pore initiates selectivity filter gating

One of the hallmarks of selectivity filter gating is its sensitivity to changes in permeant ions[25,39–42]. Further, it has been suggested that K^+ exit from the pore must precede the protein conformational changes that result in collapse of conduction[43,44]. Increases in external K^+ from 2 to 25 mM have a large effect on the rate of inactivation but relatively little effect on the rate of recovery from inactivation, and the calculated Φ value is close to 1 (**Fig. 6**). When external K^+ was increased to 100 mM, inactivation at depolarized potentials was

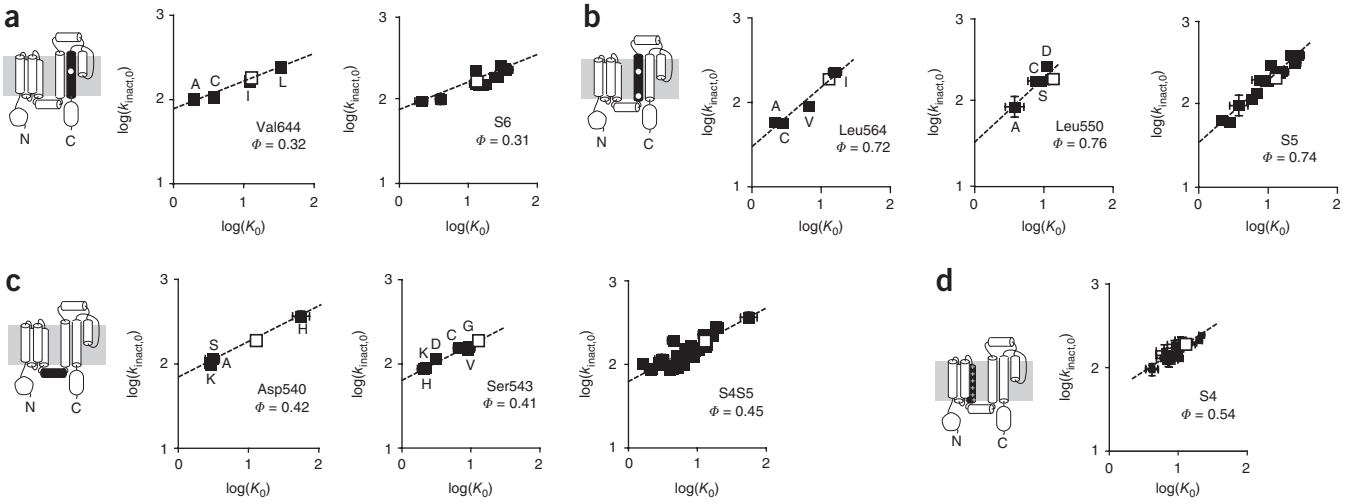

Figure 5 Mutations in transmembrane and cytoplasmic domains affect dynamics of $K_v11.1$ inactivation. Plots of $\log(k_{inact,0})$ versus $\log(K_0)$ for individual residues, where max $\Delta\log(K_0)$ is > 0.5, and summary plots for all mutants in a given domain. (**a**) S6. (**b**) S5. (**c**) S4-S5. (**d**) S4. In plots to the left of each panel, individual mutations are indicated by their single-letter amino acid codes. In each panel, the unfilled square shows WT $K_v11.1$ and error bars are ± s.e.m. for n = 4–13 oocytes. In some instances, error bars are within the symbols. White dots in the topology diagrams at far left indicate the approximate location of residues highlighted in the left panels of each row. White '+' symbols indicate approximate location of charged residues in S4 that were mutated in this study. For purposes of clarity, individual mutations are not identified in the summary panels shown at the right of each row, but the properties of all mutants examined are summarized in **Supplementary Table 1**.

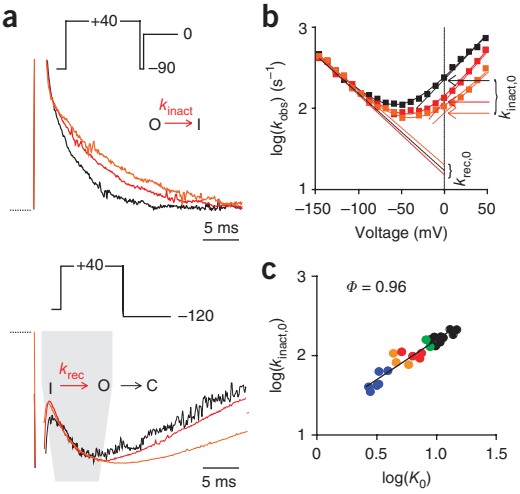

Figure 6 External K^+ concentration affects energetics of K^+ channel inactivation. (**a**) Current decay due to inactivation measured at 0 mV slows as external K^+ is increased from 2 mM K^+ (black) to 10 mM K^+ (red) and 25 mM K^+ (orange) (top). The initial increase in current due to recovery from inactivation at −120 mV (highlighted by gray shading) is relatively insensitive to changes in external K^+ (bottom). Insets show voltage protocols used to record currents. Dashed horizontal lines indicate zero current level. (**b**) Plot of the logarithm of the measured rate constants versus voltage for 2, 10 and 25 mM K^+. Dashed lines show the unilateral forward and reverse rate constants and arrows indicate $k_{inact,0}$. (**c**) Plot of $\log(k_{inact,0})$ versus $\log(K_0)$ for different external K^+ concentrations (black: 2 mM; green: 5 mM; red: 10 mM; orange: 25 mM; blue: 98 mM). Each point represents an individual experiment. The slope of the fitted line gave a Φ value of 0.96.

slowed further, but recovery from inactivation at hyperpolarized potentials was also slowed. Nevertheless, data showing the slowing of recovery from inactivation, extrapolated from the intersection of the straight line fit to the limbs of the chevron plots, are still only modestly changed at 0 mV (see **Supplementary Fig. 4**). Recent work with a KcsA-Kv1.3 chimera showed that increasing external K^+ slows the rate of inactivation without affecting the rate of recovery from inactivation[39], the same result as that seen here for inactivation of K_v11.1 K^+ channels. One interpretation for these data (scheme 1) is that K^+ exit from the outermost ion-binding site in the selectivity filter is the very first step in the transition from the open (O) to inactivated (I) states in multiple types of K^+ channels. An alternative explanation is that K^+ exit from the selectivity filter is a distinct step that precedes any conformational changes underlying the inactivation process, as described by scheme 2 below:

$$O \rightleftharpoons I \qquad \text{Scheme 1}$$

$$O_{(K)} \overset{K^+}{\rightleftharpoons} O_{(-)} \rightleftharpoons I \qquad \text{Scheme 2}$$

A Φ value of 1 in scheme 1 would indicate that K^+ exit must be the very first step in inactivation. In scheme 2, if we assume that the rate of interconversion between the K^+ occupied and K^+ empty 'open' selectivity filter is rapid relative to the conformational changes underlying inactivation, then K^+ exit would be a necessary prerequisite but not a guarantee that inactivation would take place. In such a scheme, a Φ value of 1 for K^+ exit would not necessarily indicate that this step was energetically coupled to subsequent conformational changes involved in the transition from the open to inactivated state.

DISCUSSION

Static structures have been determined by crystallography for many proteins, including for ion channels[1,5,7,45]. To fully understand how proteins work, however, we also need to determine the dynamics of the conformational changes that mediate the interconversion of stable end states[4]. In this study, we have used Φ-value analysis[9,46] to investigate the energetic coupling between different domains involved in the conformational changes[46] that link the open and inactivated states of the K_v11.1 K^+ channel, one of the best-studied examples of selectivity filter gating[18].

Φ-value analysis has been extensively applied to the analysis of protein folding reactions, where Φ values between 0 and 1 have been interpreted as indicating to what extent the protein structure, in the vicinity of a mutation, is folded or unfolded in the transition-state complex[8,9]. More recently, Φ-value analysis has been used to infer the temporal sequence of events underlying gating transitions between the closed and open states of the nicotinic acetylcholine receptor[12,13,46]. If we consider the effect of mutations on inactivation of K_v11.1 K^+ channels, our Φ-value analysis indicates that there are widespread conformational changes that start with the outer helix of the pore domain ($\Phi \sim 0.75$), followed in sequence by changes in the extracellular S5P domain ($\Phi \sim 0.6$), S4 domain ($\Phi \sim 0.55$), cytoplasmic S4-S5 domain ($\Phi \sim 0.45$) and then the inner helix of the pore domain, the linker between the pore-helix and selectivity filter, and the PS6 linker (the latter three all having Φ values of 0.25–0.3). We postulate that physical collapse of the selectivity filter will be the final step in selectivity filter gating. Unfortunately, all the mutants that we made for selectivity filter residues either were not expressed or were not amenable to analysis (see **Supplementary Table 1** for a list of all mutants examined). Therefore, this final putative step awaits experimental verification. Alternatively, one could interpret these data as indicating that in the transition state, the conformation of the outer helix of the pore domain (S5) more closely resembles the conformation of the channel in the inactivated state than it does in the open state. The S5P, S4 and S4-S5 linker domains would be more intermediate, and the structure of the inner helix of the pore domain and linkers adjacent to the selectivity filter would more closely resemble the open state structure than the inactivated state structure. Irrespective of which of these two interpretations one uses, our data clearly indicate that there are widespread conformational rearrangements of extracellular, transmembrane and cytoplasmic domains of the channel that have distinct patterns of energetic coupling to selectivity filter gating.

At this stage, the highest Φ value we have obtained for a domain motion is ~0.75 for the outer helix of the pore domain (**Fig. 4**). Given that we have restricted our analysis to open state inactivation, with the voltage sensor domains in the open configuration, and that there is strong evidence that movement of S5 is involved in the transition from the closed to open state[45], it is perfectly plausible that rearrangement of the S5 helix is a very early step in the transition from the open to inactivated states. However, we cannot rule out the possibility that there is an earlier step involved. It could be that the first step in transition from the open to inactivated states involves K^+ exit from the selectivity filter ($\Phi \sim 1$, **Fig. 6**), though it is difficult to see how K^+ exit from the pore is coupled to the conformational changes in the remainder of the channel and in particular to conformational changes in the outer helix of the pore domain (S5, Φ value ~ 0.75). If, however, we consider scheme 2, where K^+ exit from the pore is a distinct step from the conformational changes that underlie inactivation from the open state, then the probability of the channel transiting from the open (K^+ unoccupied) state to

the inactivated state would be determined by the competition between conformational changes that promote inactivation and K^+ reentry that prevents inactivation. In this scenario, there would be no need for a direct link between K^+ exit from the selectivity filter and conformational rearrangements of the channel. Further, there would be no *a priori* reason for mutants in the vicinity of the selectivity filter to have Φ values similar to those associated with perturbations caused by altering the concentration of K^+ ions.

The role of the S4 domain in inactivating $K_v11.1$ K^+ channels has been controversial[18,47]. Although the Φ value for S4 in this study (0.54) is based on measurements in which no individual mutant reaches the threshold level of $\Delta\log(K_0) > 0.5$, it is consistent with the idea that the S4 domain provides a link between movement of the extracellular turret (S5P domain) and movement of the cytoplasmic S4-S5 linker. However, it is important to note that we are studying inactivation that occurs when the voltage sensors are already in the open configuration, which is distinct from the role that movement of the S4 domain plays in activation gating. Our data are therefore consistent with the data showing that mutations in the S4 domain that affect the voltage dependence of activation have minimal effects on the voltage dependence of inactivation gating[21,48], whereas mutations in the S5P domain that affect the voltage dependence of inactivation gating have minimal effect on the voltage dependence of activation gating[30]. Our suggestion that movement of S4 is associated with inactivation raises the question as to why there are no gating current measurements that can be attributed to inactivation[21,47]. One would, however, see a gating current only if the movement of S4 occurs relative to the transmembrane electric field. If the movement of S4 is simply a rotation, as opposed to the vertical motion associated with activation, then there need not be any gating current. So the lack of gating currents associated with $K_v11.1$ inactivation[47] does not eliminate the possibility that S4 is involved in inactivation.

Φ-value analysis has previously been used to investigate the temporal sequence of domain motions underlying the closed-open state transition in the acetylcholine receptor channel[12,13,33,49]. These studies have led to the hypothesis that in ligand-gated ion channels, the sequence of conformational changes linking the closed and open states spreads in a simple wave-like manner, with the low-to-high affinity change at the transmitter-binding sites preceding the complete opening of the pore[12]. This is in marked contrast to the idea that a complex sequence of conformational changes underlies selectivity filter gating in $K_v11.1$ channels. At the very least, selectivity gating involves dynamic rearrangements of extracellular, transmembrane and intracellular domains. We propose that the mechanism of inactivation is analogous to the opening and closing of a Japanese puzzle box, in that a precise sequence of consecutive moves involving interconnected but separate elements is required to open and close an internal locking mechanism (**Fig. 7**). A plausible series of events that could explain this mechanism in $K_v11.1$ channels would be that S5 rotates and this then allows the S5P linker to translate away from the S4 domain (and thereby allows the S4 domain to move) and toward the PS6 domain. The movement of the S4 domains could initiate a rotation of the S4-S5 linker and thence a rotation of S6. Almost synchronously with this movement of S6, rearrangements of the pore-helix-selectivity filter linker and the PS6 linker ultimately lead to a putative collapse of the selectivity filter. It is important to stress that at this stage we do not have sufficient experimental data to determine the nature of the conformational changes that take place. However, there is at least some evidence in the literature to support the hypothesis that a rotation of S6 occurs during transitions between the open and inactivated states[50]. Furthermore, the data to support our placement

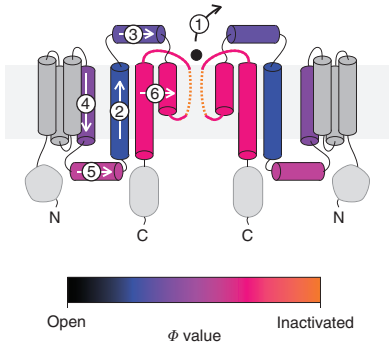

Figure 7 Japanese puzzle box model of allosteric control of selectivity filter gating. A schematic diagram showing two of the four subunits of the $K_v11.1$ channel, color coded according to whether the domain moves early (black) or late (orange) during the open to inactivated state transition as determined by Φ values derived in **Figures 3–5**. The six steps for opening the puzzle are (1) exit of K^+ ions from the external side of the selectivity filter ($\Phi \sim 1$) followed by movements of (2) the outer helix of the pore domain ($\Phi \sim 0.75$), (3) the S5P linker in the extracellular turret ($\Phi \sim 0.6$), (4) the S4 domain, (5) the cytoplasmic S4-S5 linker ($\Phi \sim 0.45$) and (6) the inner helix of the pore domain, the pore helix-selectivity filter linker and the PS6 linker (all with $\Phi \sim 0.25$). The final putative step is collapse of the selectivity filter. This final step remains to be verified experimentally. The arrows indicate the sequence of allosteric communication rather than any specific movement. The exact nature of each of the depicted domain movements remains to be determined.

of S4 ($\Phi \sim 0.55$) and the linker between the pore-helix and selectivity filter ($\Phi \sim 0.26$) in the sequence of events derives from experiments with mutants that have relatively modest $\Delta\log(K_0)$ values, and so our assignment of these domains to specific steps in the process should be considered as preliminary.

Selectivity filter gating occurs in a wide range of K^+ channels[30,31,39,43,51–53]. This raises the question as to whether the widespread conformational changes observed during selectivity filter gating in $K_v11.1$ channels are likely to be unique to this channel or conserved in other channels. In support of a unique mechanism are the observations that there are some distinct structural features in the $K_v11.1$ channel, including, for example, the much larger turret region[20,22], and the fact that the inactivation process appears to be much faster compared to, for example, Shaker[43] and KcsA[31]. Conversely, recent work showing that the conducting state of the selectivity filter in both KcsA[37] and KirBac3.1 (ref. 5) is correlated with changes in the structure of transmembrane and cytoplasmic domains is consistent with the model proposed here. It is important to note that the structural and spectroscopic methods employed in the studies of KcsA and KirBac3.1 cannot tell us anything about the dynamics of the conformational changes associated with inactivation. Application of Φ-value analysis to study selectivity filter gating in KcsA and KirBac as well as other channels could, however, answer the question as to whether the Japanese puzzle box mechanism proposed here is unique to $K_v11.1$ channels or is a more universal gating mechanism.

In this study, we have provided a 'domain level' view of the conformational changes that underlie selectivity filter gating in $K_v11.1$ channels. A more extensive high-resolution mutagenesis approach in $K_v11.1$ channels will reveal finer details of the inactivation gating process, including how clinically occurring mutations disrupt inactivation[54], as well as provide a better understanding of how drug binding to the $K_v11.1$ channel is affected by the conformational state of the selectivity filter[16].

METHODS

Methods and any associated references are available in the online version of the paper at http://www.nature.com/nsmb/.

Note: Supplementary information is available on the Nature Structural & Molecular Biology website.

ACKNOWLEDGMENTS

We thank E. Perozo for providing preprints of papers in press; R.M Graham, A. Husain, L. Lee, B. Martinac, E. Perozo and M. Sunde for participating in critical discussions and for reading the manuscript; and K. Wyse and T. Marciniec for making technical contributions. This research was supported by project grants from the National Health and Medical Research Council of Australia (NHMRC, grants 459402 and 635520) and fellowships to J.V. (NHMRC grant 459401) and to A.H. (National Heart Foundation of Australia grant PF 08S 3956).

COMPETING FINANCIAL INTERESTS

The authors declare no competing financial interests.

Published online at http://www.nature.com/nsmb/.
Reprints and permissions information is available online at http://npg.nature.com/reprintsandpermissions/.

1. Doyle, D.A. *et al.* The structure of the potassium channel: molecular basis of K^+ conduction and selectivity. *Science* **280**, 69–77 (1998).
2. Yellen, G. The voltage-gated potassium channels and their relatives. *Nature* **419**, 35–42 (2002).
3. Bernèche, S. & Roux, B. A gate in the selectivity filter of potassium channels. *Structure* **13**, 591–600 (2005).
4. Henzler-Wildman, K. & Kern, D. Dynamic personalities of proteins. *Nature* **450**, 964–972 (2007).
5. Clarke, O.B. *et al.* Domain reorientation and rotation of an intracellular assembly regulate conduction in Kir potassium channels. *Cell* **141**, 1018–1029 (2010).
6. Cuello, L.G., Jogini, V., Cortes, D.M. & Perozo, E. Structural mechanism of C-type inactivation in K^+ channels. *Nature* **466**, 203–208 (2010).
7. Long, S.B., Tao, X., Campbell, E.B. & MacKinnon, R. Atomic structure of a voltage-dependent K^+ channel in a lipid membrane-like environment. *Nature* **450**, 376–382 (2007).
8. Fersht, A.R. From the first protein structures to our current knowledge of protein folding: delights and scepticisms. *Nat. Rev. Mol. Cell Biol.* **9**, 650–654 (2008).
9. Fersht, A.R., Leatherbarrow, R.J. & Wells, T.N.C. Quantitative analysis of structure-activity relationships in engineered proteins by linear free-energy relationships. *Nature* **322**, 284–286 (1986).
10. Fersht, A.R., Matouschek, A. & Serrano, L. The folding of an enzyme. I. Theory of protein engineering analysis of stability and pathway of protein folding. *J. Mol. Biol.* **224**, 771–782 (1992).
11. Fersht, A.R. Relationship of Leffler (Bronsted) alpha values and protein folding Phi values to position of transition-state structures on reaction coordinates. *Proc. Natl. Acad. Sci. USA* **101**, 14338–14342 (2004).
12. Grosman, C., Zhou, M. & Auerbach, A. Mapping the conformational wave of acetylcholine receptor channel gating. *Nature* **403**, 773–776 (2000).
13. Purohit, P., Mitra, A. & Auerbach, A. A stepwise mechanism for acetylcholine receptor channel gating. *Nature* **446**, 930–933 (2007).
14. Zhou, Y., Pearson, J.E. & Auerbach, A. Phi-value analysis of a linear, sequential reaction mechanism: theory and application to ion channel gating. *Biophys. J.* **89**, 3680–3685 (2005).
15. Sanguinetti, M.C. & Tristani-Firouzi, M. hERG potassium channels and cardiac arrhythmia. *Nature* **440**, 463–469 (2006).
16. Perrin, M.J., Kuchel, P.W., Campbell, T.J. & Vandenberg, J.I. Drug binding to the inactivated state is necessary but not sufficient for high-affinity binding to human ether-a-go-go-related gene channels. *Mol. Pharmacol.* **74**, 1443–1452 (2008).
17. Smith, P.L., Baukrowitz, T. & Yellen, G. The inward rectification mechanism of the HERG cardiac potassium channel. *Nature* **379**, 833–836 (1996).
18. Vandenberg, J.I., Torres, A.M., Campbell, T.J. & Kuchel, P.W. The HERG K^+ channel: progress in understanding the molecular basis of its unusual gating kinetics. *Eur. Biophys. J.* **33**, 89–97 (2004).
19. Ju, P. *et al.* The pore domain outer helix contributes to both activation and inactivation of the HERG K^+ channel. *J. Biol. Chem.* **284**, 1000–1008 (2009).
20. Liu, J., Zhang, M., Jiang, M. & Tseng, G.N. Structural and functional role of the extracellular s5-p linker in the HERG potassium channel. *J. Gen. Physiol.* **120**, 723–737 (2002).
21. Piper, D.R., Hinz, W.A., Tallurri, C.K., Sanguinetti, M.C. & Tristani-Firouzi, M. Regional specificity of human ether-a-go-go-related gene channel activation and inactivation gating. *J. Biol. Chem.* **280**, 7206–7217 (2005).
22. Torres, A.M. *et al.* Structure of the HERG K^+ channel S5P extracellular linker: role of an amphipathic alpha-helix in C-type inactivation. *J. Biol. Chem.* **278**, 42136–42148 (2003).
23. Zou, A., Xu, Q.P. & Sanguinetti, M.C. A mutation in the pore region of HERG K^+ channels expressed in *Xenopus* oocytes reduces rectification by shifting the voltage dependence of inactivation. *J. Physiol. (Lond.)* **509**, 129–137 (1998).
24. Sanguinetti, M.C., Jiang, C., Curran, M.E. & Keating, M.T. A mechanistic link between an inherited and an acquired cardiac arrhythmia: HERG encodes the IKr potassium channel. *Cell* **81**, 299–307 (1995).
25. Wang, S., Liu, S., Morales, M.J., Strauss, H.C. & Rasmusson, R.L. A quantitative analysis of the activation and inactivation kinetics of HERG expressed in *Xenopus* oocytes. *J. Physiol. (Lond.)* **502**, 45–60 (1997).
26. Kiehn, J., Lacerda, A.E. & Brown, A.M. Pathways of HERG inactivation. *Am. J. Physiol.* **277**, H199–H210 (1999).
27. Gang, H. & Zhang, S. Na^+ permeation and block of hERG potassium channels. *J. Gen. Physiol.* **128**, 55–71 (2006).
28. Zou, A., Curran, M.E., Keating, M.T. & Sanguinetti, M.C. Single HERG delayed rectifier K^+ channels expressed in *Xenopus* oocytes. *Am. J. Physiol.* **272**, H1309–H1314 (1997).
29. Jackson, S.E. & Fersht, A.R. Folding of chymotrypsin inhibitor 2. 1. Evidence for a two-state transition. *Biochemistry* **30**, 10428–10435 (1991).
30. Clarke, C.E. *et al.* Effect of S5P alpha-helix charge mutants on inactivation of hERG K^+ channels. *J. Physiol. (Lond.)* **573**, 291–304 (2006).
31. Cordero-Morales, J.F. *et al.* Molecular driving forces determining potassium channel slow inactivation. *Nat. Struct. Mol. Biol.* **14**, 1062–1069 (2007).
32. Liu, Y., Jurman, M.E. & Yellen, G. Dynamic rearrangement of the outer mouth of a K^+ channel during gating. *Neuron* **16**, 859–867 (1996).
33. Cymes, G.D., Grosman, C. & Auerbach, A. Structure of the transition state of gating in the acetylcholine receptor channel pore: a phi-value analysis. *Biochemistry* **41**, 5548–5555 (2002).
34. Yellen, G., Sodickson, D., Chen, T.Y. & Jurman, M.E. An engineered cysteine in the external mouth of a K^+ channel allows inactivation to be modulated by metal binding. *Biophys. J.* **66**, 1068–1075 (1994).
35. Fersht, A.R., Leatherbarrow, R.J. & Wells, T.N. Structure-activity relationships in engineered proteins: analysis of use of binding energy by linear free energy relationships. *Biochemistry* **26**, 6030–6038 (1987).
36. Ozkan, S.B., Bahar, I. & Dill, K.A. Transition states and the meaning of Phi-values in protein folding kinetics. *Nat. Struct. Biol.* **8**, 765–769 (2001).
37. Cuello, L.G. *et al.* Structural basis for the coupling between activation and inactivation gates in K^+ channels. *Nature* **466**, 272–275 (2010).
38. Ferrer, T., Rupp, J., Piper, D.R. & Tristani-Firouzi, M. The S4-S5 linker directly couples voltage sensor movement to the activation gate in the human ether-a-go-go-related gene (hERG) K^+ channel. *J. Biol. Chem.* **281**, 12858–12864 (2006).
39. Ader, C. *et al.* Coupling of activation and inactivation gate in a K^+-channel: potassium and ligand sensitivity. *EMBO J.* **28**, 2825–2834 (2009).
40. Baukrowitz, T. & Yellen, G. Modulation of K^+ current by frequency and external $[K^+]$: a tale of two inactivation mechanisms. *Neuron* **15**, 951–960 (1995).
41. Cordero-Morales, J.F. *et al.* Molecular determinants of gating at the potassium-channel selectivity filter. *Nat. Struct. Mol. Biol.* **13**, 311–318 (2006).
42. López-Barneo, J., Hoshi, T., Heinemann, S.H. & Aldrich, R.W. Effects of external cations and mutations in the pore region on C-type inactivation of Shaker potassium channels. *Receptors Channels* **1**, 61–71 (1993).
43. Baukrowitz, T. & Yellen, G. Use-dependent blockers and exit rate of the last ion from the multi-ion pore of a K^+ channel. *Science* **271**, 653–656 (1996).
44. Ogielska, E.M. & Aldrich, R.W. Functional consequences of a decreased potassium affinity in a potassium channel pore. Ion interactions and C-type inactivation. *J. Gen. Physiol.* **113**, 347–358 (1999).
45. Jiang, Y. *et al.* The open pore conformation of potassium channels. *Nature* **417**, 523–526 (2002).
46. Auerbach, A. How to turn the reaction coordinate into time. *J. Gen. Physiol.* **130**, 543–546 (2007).
47. Piper, D.R., Varghese, A., Sanguinetti, M.C. & Tristani-Firouzi, M. Gating currents associated with intramembrane charge displacement in HERG potassium channels. *Proc. Natl. Acad. Sci. USA* **100**, 10534–10539 (2003).
48. Subbiah, R.N. *et al.* Molecular basis of slow activation of the human ether-a-go-go related gene potassium channel. *J. Physiol. (Lond.)* **558**, 417–431 (2004).
49. Bafna, P.A., Jha, A. & Auerbach, A. Aromatic residues {epsilon}Trp-55 and {delta}Trp-57 and the activation of acetylcholine receptor channels. *J. Biol. Chem.* **284**, 8582–8588 (2009).
50. Chen, J., Seebohm, G. & Sanguinetti, M.C. Position of aromatic residues in the S6 domain, not inactivation, dictates cisapride sensitivity of HERG and eag potassium channels. *Proc. Natl. Acad. Sci. USA* **99**, 12461–12466 (2002).
51. Kurata, H.T. & Fedida, D. A structural interpretation of voltage-gated potassium channel inactivation. *Prog. Biophys. Mol. Biol.* **92**, 185–208 (2006).
52. Larsson, H.P. & Elinder, F. A conserved glutamate is important for slow inactivation in K^+ channels. *Neuron* **27**, 573–583 (2000).
53. Panyi, G. & Deutsch, C. Cross talk between activation and slow inactivation gates of Shaker potassium channels. *J. Gen. Physiol.* **128**, 547–559 (2006).
54. Zhao, J.T. *et al.* Not all hERG pore domain mutations have a severe phenotype: G584S has an inactivation gating defect with mild phenotype compared to G572S, which has a dominant negative trafficking defect and a severe phenotype. *J. Cardiovasc. Electrophysiol.* **20**, 923–930 (2009).

ONLINE METHODS

Mutagenesis and expression. K_v11.1 cDNA (a gift from G. Robertson, University of Wisconsin, Madison) was subcloned into a pBluescript vector containing the 5′ untranslated region (UTR) and 3′ UTR of the *Xenopus laevis* β-globin gene (a gift from R. Vandenberg, University of Sydney). Mutagenesis was carried out on a BstEII-BglII fragment (bp 1119–1937) of K_v11.1 using the megaprimer PCR method as previously described[30]. In some cases, mutant generation was outsourced to Mutagenex. cRNA was synthesized, after linearization of the plasmid with BamHI, using the mMessage mMachine kit (Ambion) according to the manufacturer's protocols.

Electrophysiology. Female *X. laevis* frogs were purchased from Nasco. Oocytes were prepared as previously described[30]. The Garvan/St. Vincent's Animal Ethics Committee approved all experiments. All experiments were undertaken at room temperature (21–22 °C). Oocytes were perfused with ND96 solution (96 mM NaCl, 2 mM KCl, 1.8 mM $CaCl_2$, 1 mM $MgCl_2$, 5 mM HEPES, pH 7.5) at a rate of ~2 ml min^{-1}. In high-K^+ solutions, KCl was substituted for an equivalent amount of NaCl. Glass microelectrodes had tip resistances of 0.2–1.0 MΩ when filled with 3 M KCl. Data analysis was done using pClamp software (Version 9.2, Molecular Devices) and Excel software (Microsoft Corporation). All data are shown as mean ± s.e.m.

Rate constant determination. Rates of inactivation were determined from a triple-pulse voltage protocol[55] (see **Fig. 2a**). Cells were first depolarized to +40 mV for 500 ms to ensure channels were fully activated and inactivated. For some mutants, it was necessary to use a step to +80 or +120 mV to ensure full inactivation. The voltage was then stepped to −90 mV to enable the channels to recover from inactivation into the open state. The specific duration of the second step was varied depending on the rate of deactivation of the different mutants. The potential was then stepped to varying depolarized voltages and the rate of reentry into the inactivated state monitored.

A two-step voltage protocol was used to measure rates of recovery from inactivation[55] (see **Fig. 2a**). Cells were initially depolarized to +40 mV for 500 ms to fully inactivate the channels, followed by steps to more negative voltages to allow the channels to recover from the inactivated state into the open state.

The rates of inactivation and recovery from inactivation were obtained by fitting an exponential function to the relevant portion of the current trace. Where there was appreciable deactivation occurring before complete recovery from inactivation, a double exponential was fitted to the current trace[55].

The unilateral forward (k_{inact}) and backward (k_{rec}) rate constants are related to the observed rate ($k_{obs,V}$) constants by equation (3):

$$k_{obs,V} = k_{inact,V} + k_{rec,V} \quad (3)$$

In this study we used the derived values for $k_{inact,V}$ and $k_{rec,V}$ at 0 mV to calculate the equilibrium constant K at 0 mV:

$$K_0 = k_{inact,0} / k_{rec,0} \quad (4)$$

Equilibrium values were also calculated from the ratio of steady-state current to peak current during triple-pulse voltage protocols (**Fig. 2a**). Equilibrium values obtained for the two different methods were very similar (**Fig. 2c** and **Supplementary Fig. 1**).

Calculation of Φ values. A Φ value represents the ratio of the perturbation to the energetics of the transition state relative to the energetics of the ground states[10] (open and inactivated in the case of K_v11.1 channel inactivation, see **Fig. 1**):

$$\Phi = \Delta\Delta G^{\ddagger} / \Delta\Delta G^{0} \quad (5a)$$

Given that:

$$\Delta G^{\ddagger} = -RT\ln(k_{inact}) \text{ and } \Delta G^{0} = -RT\ln(K)$$

where R is the universal gas constant and T is temperature, then

$$\Phi = -RT\,\Delta\ln(k_{inact}) / -RT\,\Delta\ln(K) = \Delta\log(k_{inact}) / \Delta\log(K) \quad (5b)$$

Φ values were calculated either from the slope of a straight line fit to a plot of $\log(k_{inact,0})$ versus $\log(K_0)$ for all the mutants at a given residue or domain[10,46] (see **Figs. 3–5**) or directly from the values for $\log(k_{inact,0})$ and $\log(K_0)$ for individual pairs of mutants using equation (5b) (see **Fig. 3c**). It is important to note that when $\Delta\log(K_0)$ is small, even small errors in the measurement of $\Delta\log(K_0)$ can lead to large errors in the calculated Φ value. As can be seen from **Figure 3d**, we found that $\Delta\log(K_0)$ needs to be >0.5 to obtain an accurate estimate of Φ values. This is similar to the cutoff value determined for Φ-value analysis of the acetylcholine receptor[33].

55. Vandenberg, J.I. *et al.* Temperature dependence of human ether-a-go-go-related gene K^+ currents. *Am. J. Physiol. Cell Physiol.* **291**, C165–C175 (2006).

doi:10.1038/nsmb.1966